minerals

MDPI

Article

Properties of Inorganic Polymers Produced from Brick Waste and Metallurgical Slag

Athanasia Soultana [1], Aikaterini Valouma [2], Georgios Bartzas [3] and Konstantinos Komnitsas [1,*]

1 School of Mineral Resources Engineering, Technical University of Crete, 73100 Chania, Greece; nansoula21@hotmail.com
2 School of Environmental Engineering, Technical University of Crete, 73100 Chania, Greece; avalouma@gmail.com
3 School of Mining and Metallurgical Engineering, National Technical University of Athens, 15780 Zografos, Greece; gbartzas@metal.ntua.gr
* Correspondence: komni@mred.tuc.gr; Tel.: +30-28210-37686

Received: 8 July 2019; Accepted: 9 September 2019; Published: 12 September 2019

Abstract: This paper explores the alkali activation potential of brick wastes and metallurgical slags. Inorganic polymers (IPs) were produced using an alkaline medium consisting of sodium hydroxide and sodium silicate solutions and the optimum synthesis conditions were determined. In this context, the variable parameters, such as solid to liquid (S/L) ratio, curing temperature (60, 80 and 90 °C) and ageing time (7 and 28 days) on the compressive strength and the morphology of the produced IPs were investigated. Specimens produced under the optimum synthesis conditions were subjected to high temperature firing and immersed in distilled water and acidic solutions for various periods of time, in order to assess their durability and structural integrity. The results showed that the IPs produced using a mix ratio of 50 wt % metallurgical slag and 50 wt % brick wastes, cured at 90 °C and aged for 7 days obtained the highest compressive strength (48.9 MPa). X-ray fluorescence analysis (XRF), particle size analysis, Fourier transform infrared spectroscopy (FTIR), mineralogical analysis (XRD), mercury intrusion porosimetry (MIP), scanning electron microscopy (SEM) and thermogravimetric (TG) analysis also confirmed the optimum microstructural characteristics and the chemical reactions that took place during synthesis. The overall results of this study indicate that the co-valorization of different waste streams, which are produced in large quantities and cause environmental problems if not properly managed, is a viable alternative for the production of binders or secondary construction materials with higher added value.

Keywords: inorganic polymers (IPs); brick waste; metallurgical slag; compressive strength

1. Introduction

Construction and demolition wastes (CDWs) comprise the largest waste fraction in industrialized countries. They represent one third of the total waste volume generated by industrial activities, which in the EU-28 is about 3 billion tons per year [1]. CDWs derive from construction and demolition activities and mainly contain concrete, masonry, asphalt and metals [2]. It is estimated that approximately 54% of CDW is comprised of ceramic materials (i.e., bricks and tiles), while approximately 12% is concrete [3]. Their disposal requires large areas and often causes severe impacts to the environment [1,4]. On the other hand, the energy requirements for the production of concrete are almost 5% of the global energy consumption. Moreover, the production of 1 ton of cement results in emissions of approximately 1 ton of carbon dioxide (CO_2), while aggregate production also poses severe problems to surrounding areas [2,5,6].

In recent years, a large number of studies pertinent to the recycling of CDW and the production of eco-friendly concrete have been carried out. A promising alternative for the management of CDW appears to be alkali-activation for the production of secondary materials, often called inorganic polymers (IPs) or geopolymers. These materials exhibit advanced physico-chemical properties, including good fire and chemical resistance, and can be used in the construction sector [4,7,8]. IPs are synthesized by using various wastes and alkaline solutions [6,7,9–11]. The alkaline solutions, mainly sodium or potassium hydroxide and silicate solutions, act as activators to initiate polymerization of Si and Al present in the raw materials and for the formation of Si–O–Al–O bonds [12]. Raw materials rich in silica and alumina, including bricks, ceramic waste, metakaolin, fly ash, kaolin and slag can be used for the production of IPs [2,12]. Apart from the construction sector, the produced IPs may be used for the immobilization of hazardous elements or as adsorbents in various industrial processes [13–17]. The properties of the produced IPs may be determined by the use of various analytical techniques [3,18].

Alkaline activation has been recently attracted attention as a promising option for the management of CDW and the production of IPs with beneficial mechanical, thermal and physico-chemical properties [19,20]. Apart from the use of single CDW constituents, other waste streams, such as slags, leaching residues and sediments may be used in order to obtain optimum raw material mixtures and IPs with tailored properties [15,20–22]. The degree of reactivity of each waste stream differs and depends on the type and content of the contained aluminosilicates. More details on the reactivity of a wide range of natural Al–Si minerals that could serve as potential source materials for the synthesis of geopolymers can be found in an excellent earlier study [23].

Slag is a brittle material with varying grain size (0.075–4 mm). Large amounts of slags are produced worldwide as by-products of steel and non-ferrous metal production. Part of the produced slag, namely ground granulated blast-furnace slag (GGBFS), is used in the cement industry, while the remaining quantities are disposed of in various sites. Improper disposal practices may result in solubilization of the contained hazardous elements and cause damage to environmental receptors [24,25]. Valorization of metallurgical slags through alkali-activation appears to be a viable management option [20,26]. The role of iron during alkali activation of iron-rich raw materials for the production of geopolymers has been investigated in previous studies and the results are often contradictory. It has been indicated that possible incorporation of ferric iron in the tetrahedral network of geopolymers may result in products with increased strength. In such systems, the behavior or iron can be elucidated through ^{57}Fe Mössbauer spectroscopy and/or *in-situ* X-ray total scattering and subsequent pair distribution function analysis. The results of these investigations may also predict the long-term behavior of the produced geopolymers [9,27–29].

The co-valorization of different waste streams is in line with the principles of industrial symbiosis and circular economy [30,31]. Thus, this research study aims to fully investigate the optimum alkali-activation synthesis conditions and the associated properties of IPs produced using brick wastes and metallurgical slag as raw materials. In this context, several factors have been studied, including oxide molar ratios in the initial paste, and curing and ageing conditions.

2. Materials and Methods

Brick wastes, clean of other contaminants, such as concrete, collected from demolished buildings (Chania, Crete, Greece), and metallurgical slag (S), produced during ferronickel production at the "LARCO S.A" plant (Larymna, Central Greece), were used for the production of IPs. Brick waste was pulverized using a Sepor type rod mill (5" Series, Sepor, Los Angeles, CA, USA), while metallurgical slag was with the use of a Bico type pulverizer (Type UA, Fritsch, Dresden, Germany). Chemical composition in the form of oxides was determined using an X-ray fluorescence energy dispersive spectrometer (XRF-EDS) (Bruker AXS (D8 Advance type), Bruker, Karlsruhe, Germany), Bruker-AXS S2 Range type (Bruker, Karlsruhe, Germany). Loss on ignition (LOI) was determined by heating the materials at 1050 °C for 4 h and particle size analysis of the raw materials was determined by a laser particle size

analyzer (Mastersizer S, Malvern Instruments, Malvern, UK). The chemical composition and particle size distribution of the raw materials used are presented in Table 1.

Table 1. Chemical analysis and particle size distribution of raw materials.

Chemical Composition (wt %)	Bricks	Slag
SiO_2	59.1	32.7
CaO	17.8	3.7
Al_2O_3	10.2	8.3
MgO	1.9	2.8
K_2O	1.9	-
Fe_2O_3	7.4	43.8
Cr_2O_3	-	3.1
TiO_2	1.0	-
MnO	0.1	0.4
SO_3	-	0.5
LOI	0.2	-
Total	99.6	95.3
Particle Size Distribution (%)		
d_{90} (μm)	94.3	45.6
d_{50} (μm)	16.7	8.9
d_{10} (μm)	0.5	0.4

LOI: Loss on ignition.

It is observable from this table that both raw materials contain high amounts of SiO_2 (59.1 and 32.7 wt % for brick and slag, respectively) and Al_2O_3 (10.2 and 3.7 wt % for brick and slag, respectively) which indicates their potential for alkali activation. Furthermore, the CaO content in bricks is much higher compared to slag (17.8 and 3.7 wt %, respectively), while the Fe_2O_3 content in slag (43.8 wt %) is almost six times higher than the respective content in brick waste (7.4 wt %). The main mineralogical phases present in brick waste are quartz (SiO_2) and calcite ($CaCO_3$), while slag is mostly dominated by iron oxides and quartz [9,20].

The mixing proportions used for the synthesis of IPs are shown in Table 2. The activating solution used consisted of sodium hydroxide solution, 6–10 mol L^{-1} (M), produced by dissolving the required amount of NaOH anhydrous pellets in distilled water and sodium silicate solution (Na_2O = 7.5–8.5 wt %, SiO_2 = 25.5–28.5 wt %). Sodium hydroxide was selected over potassium hydroxide solution, since the IPs produced during preliminary tests obtained better mechanical properties. It has been shown in earlier studies carried out in our laboratory that the use of NaOH solution causes higher Si and Al dissolution from similar raw materials [20]. The effect of different H_2O/Na_2O (15.5, 18.1 and 22.0) and SiO_2/Na_2O molar ratios (1.0, 1.2 and 1.4) in the activating solution was also investigated and is shown in Table 2.

Table 2. Mixing proportions of raw materials and solutions (wt %).

IP Code [1]	NaOH (M)	Solids (S)		Liquids (L)					S/L Ratio
		Brick	Slag	NaOH	H_2O	Na_2SiO_3	H_2O/Na_2O Molar Ratio	SiO_2/Na_2O Molar Ratio	
B6	6	70.9	-	2.6	10.4	16.1	22.0	1.4	2.4
B8	8	71.4	-	3.2	9.5	15.9	18.1	1.2	2.5
B10	10	69.0	-	4.2	9.6	17.2	15.5	1.0	2.2
S	8	-	81.1	2.1	6.3	10.5	18.1	1.2	4.3
B75S25	8	56.3	18.8	2.8	8.3	13.8	18.1	1.2	3.0
B50S50	8	38.2	38.2	2.7	7.8	13.1	18.1	1.2	3.2

[1] Abbreviations: B6: Brick, 6 M NaOH; S: Slag; B75S25: Brick 75 wt % and Slag 25 wt %.

First, raw materials were mixed with the activating solution in a laboratory mixer for 15 min so that a homogeneous paste was obtained. Then, the paste was cast in cubic steel molds 5 × 5 × 5 cm^3. The molds were vibrated for 5 min to eliminate the presence of air voids within the reactive paste and then remained at room temperature for either 6 h (brick-based specimens) or 24 h (brick-slag specimens) to enable hardening of the paste, which mainly depends on the amount of water present, the particle

size of the raw materials and the strength of the activating solution. Specimens were then demolded, sealed in plastic bags to avoid evaporation of water and heated at 60, 80 and 90 °C for 24 h in an oven (ON-02G). After an ageing period of 7 or 28 days, the compressive strength of the produced IPs was determined using a Matest type compression and flexural machine (C123N, Matest S.p.A, Treviolo, Bergamo, Italy) with dual range 500/15 kN. The experimental conditions used were based on previous studies carried out in the laboratory for the production of IPs with the use of various industrial wastes [13,32]. In each test, the solid to liquid (S/L) ratio was slightly modified so that a paste with proper flowability was produced; solids include the raw materials while liquids include the activating solution (NaOH solution of a given molarity and Na_2SiO_3 solution). Tests and measurements were carried out in triplicate and mean values are given in the following tables and figures.

The produced IPs were characterized using analytical techniques such as X-ray Diffraction (XRD), Fourier transform infrared spectroscopy (FTIR), mercury intrusion porosimetry (MIP), thermogravimetric (TG) analysis and scanning electron microscopy (SEM). XRD analysis was performed using an X-ray diffractometer (Bruker AXS, D8-Advance, Bruker, Karlsruhe, Germany) with a Cu tube and a scanning range from 4° to 70° 2theta (θ), with a step of 0.02°, and 0.2 s/step measuring time. Qualitative analysis was carried out using the DiffracPlus Software (EVA v. 2006\, Bruker, Karlsruhe, Germany) and the PDF database. FTIR analysis was carried out on KBr pellets with a PerkinElmer 1000 spectrometer (PerkinElmer, Akron, OH, USA), in the spectra range of 400 to 4000 cm^{-1}. Pellets were produced by mixing each sample with KBr at a ratio 1:100 wt %. The porosity (%) of selected specimens was determined using a Micromeritics AutoPore 9400 porosimeter (Micromeritics, Atlanta, GA, USA). Water absorption of selected specimens was determined according to EN 13755 [33]. Thermogravimetric analysis was performed up to a maximum temperature of 900 °C, using a heating rate 10 °C/min and a nitrogen atmosphere with a 100 mL/min flow rate. Scanning electron microscopy (SEM) was carried out to evaluate the morphology of the raw materials and the IPs produced. Specimens were evaluated under low-vacuum mode using a JEOL-6380LV scanning microscope (JEOL Ltd., Tokyo, Japan) equipped with an Oxford INCA energy dispersive spectroscopy (EDS) microanalysis system (Oxford Instruments, Abingdon, UK) for elemental analysis.

IPs produced under the optimum synthesis conditions were then subjected to firing at 400, 600 and 800 °C for 1 h, using a laboratory furnace (N-8L Selecta) and also immersed in various solutions, namely distilled water and acidic solutions (1 M HCl and 1 M H_2SO_4) for a period of 7 and 30 days, to assess their durability in different environments. Compressive strength, weight loss and volumetric shrinkage of the IPs were also determined.

3. Results

3.1. Effect of H_2O/Na_2O Molar Ratio in the Activating Solutions and Curing Temperatures on the Compressive Strength

The compressive strength of the IPs produced from brick waste (B) as a function of H_2O/Na_2O molar ratio in activating solutions (15.5, 18.1 and 22.0) and curing temperatures (60, 80 and 90 °C) is illustrated in Figure 1. This figure also shows, for comparison, the compressive strength of slag control specimens (S) produced with H_2O/Na_2O molar ratio equal to 18.1. It can be seen that, as the H_2O/Na_2O molar ratio increases from 15.5 to 18.1; the compressive strength of specimens cured at high temperature (80 and 90 °C) also increases whereas, the same increase in H_2O/Na_2O molar ratio, resulted in lower compressive strength for specimens cured at the lower temperature (60 °C). A further increase in H_2O/Na_2O molar ratio from 18.1 to 22.0, resulted in reduced values of compressive strength for all brick-based IPs. High content of Na_2O causes a reduction of compressive strength due to the presence of excessive hydroxyl ions in the reactive paste, some of which remain unreacted [26]. The positive effect of higher curing temperature on the compressive strength of the produced IPs can be attributed to the fact that the alkaline activation at elevated temperatures accelerates dissolution of aluminosilicates present in raw materials and enables the formation of stronger bonds, as indicated in previous studies using similar raw materials [18,20,29]. The maximum values of compressive

strength were obtained for the IPs synthesized from brick waste when the H_2O/Na_2O ratio was 18.1, after curing at 90 °C and ageing for 7 days. Finally, it is seen that the compressive strength of slag-based IPs is higher in all cases, due to the beneficial properties of slag, which has an amorphous content that exceeds 50%, as indicated in several previous studies [9,18,20].

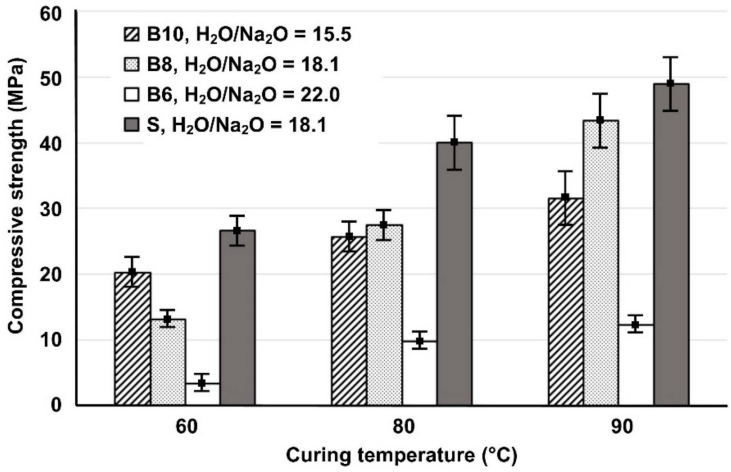

Figure 1. Effect of the H_2O/Na_2O molar ratio in the activating solutions and curing temperatures on the 7-day compressive strength of brick-and slag-based inorganic polymers (IPs) (Error bars represent the standard deviation of three measurements).

3.2. The Effects of Molar Ratios of Oxides in the Initial Paste

In order to better explain the role of synthesis conditions on the alkali activation potential of the raw materials tested, the effect of the selected molar ratios of oxide in the initial paste on the compressive strength of the produced IPs was investigated. It was seen (Table 3) that although bricks and slag can be successfully alkali-activated, brick-based specimens (B) obtained lower compressive strength. As already mentioned, the H_2O/Na_2O molar ratio in activating solution is a crucial factor that defines the strength of the produced IPs. Also, the $(SiO_2 + Al_2O_3)/Na_2O$ ratio in the reactive paste obtains an optimum value (Figure 2) which results in the highest compressive strength, due to the higher degree of hydrolysis and dissolution of Si and Al that polymerize and polycondensate. Higher or lower ratios indicate deficiency or excess of the activating solution and normally result in the production of IPs with lower compressive strength [34]. To be mentioned here also, is that the application of mild manual pressure on the paste during casting results in specimens with increased compressive strength. For example, the compressive strength of the specimen B50S50 reached 66.7 MPa, 36% higher compared to the value obtained (48.9 MPa) after normal casting.

Table 3. The effect of selected oxide molar ratios in the initial paste on the compressive strength of selected IPs.

Code	Compressive Strength [1] (MPa)	Molar Ratios		
		SiO_2/Al_2O_3	$(SiO_2 + Al_2O_3)/Na_2O$	H_2O/Na_2O
S	49.0	7.4	14.0	18.3
B6 [2]	12.3	10.8	15.8	21.8
B8	43.4	10.9	14.0	18.2
B10	31.5	11.0	11.0	15.5
B75S25	45.2	10.1	15.0	18.2
B50S50	48.9	9.3	14.0	17.9

[1] Measured after 7 days, curing temperature 90 °C; [2] B: brick-based IP after alkali activation with 6 M NaOH.

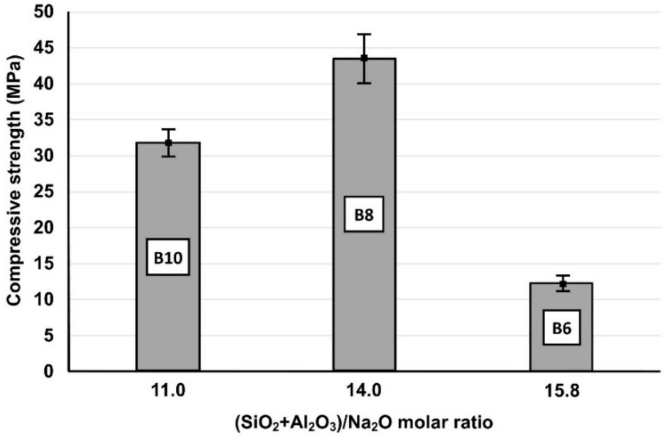

Figure 2. Effect of (SiO_2 + Al_2O_3)/Na_2O molar ratio in the reactive paste on the 7-day compressive strength of brick-based IPs (B6, B8 and B10) cured at 90 °C (Error bars represent the standard deviation of three measurements).

Moreover, it can be observed that IPs produced from mixtures rich in Al_2O_3, thus with lower SiO_2/Al_2O_3 and higher (SiO_2 + Al_2O_3)/Na_2O ratios respectively, such as the specimens S (slag) and B50S50, obtained higher compressive strength, since, besides SiO_2, higher content of Al_2O_3 in the reactive paste promotes alkali activation reactions [35]. The actual required amounts of SiO_2 and Al_2O_3 for these reactions differ and depend on the reactivity of the mineralogical phases present in the raw materials. Both brick-slag IPs (B75S25 and B50S50) obtained high compressive strength (>45 MPa) due to the increased reactivity of slag [36]. We will also mention that apart from the amorphous content, the geopolymerization of iron-rich raw materials with lower Ca content results in the formation of a stronger bonding network due to the formation of Fe–O–Si–O–Fe linkages [29,37]; in our case, the content of Ca in the raw materials used for the production of B50S50 is lower compared to the respective Ca content in the mixture used for the production of B75S50.

Figure 3 shows the compressive strength of IPs produced from brick waste and metallurgical slag using mixing ratios of 75:25 and 50:50 wt % (B75S25 and B50S50, respectively), as a function of ageing time; the strength of the control specimens, B8 and S respectively, is also given for comparison. In general, it can be observed that the increase in ageing time from 7 to 28 days has a minor effect on the compressive strength of all produced IPs; this indicates that alkali activation reactions proceed quickly and both the pre-curing and curing periods used are considered adequate.

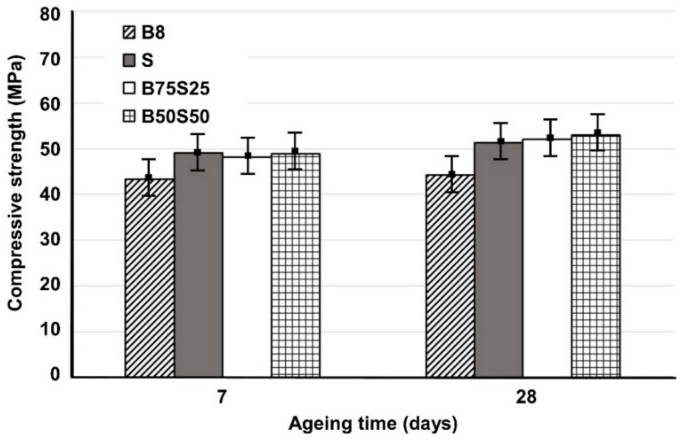

Figure 3. Compressive strength of B8, S (slag), B75S25 and B50S50 IPs produced under the optimum conditions (H_2O/Na_2O = 18.2, curing at 90 °C) as a function of ageing time (error bars represent the standard deviation of three measurements).

Table 4 shows the values of water absorption, porosity and density of selected IPs, namely the control B8 and S, and the B50S50 specimens. It can be seen that the values of these properties for B50S50 IP are almost the average of the respective values of B8 and S specimens. It is also deduced that the compressive strength of all three specimens is only slightly affected by the range of these values.

Table 4. Physical properties of selected specimens (H_2O/Na_2O = 18.2, curing at 90 °C and ageing for 7 days).

Code	Compressive Strength (MPa)	Water Absorption (%)	Porosity (%)	Density (kg/m^3)
B8	43.4	22.2	26.5	2020
S	49.0	4.2	10.8	2580
B50S50	48.9	11.3	16.7	2100

Table 5 compares the results obtained in this study with those derived from other selected studies regarding the alkali activation of brick wastes or mixtures of brick wastes and other raw materials.

Table 5. Comparison of compressive strength for brick-waste based IPs.

Raw Materials [1]	Na_2O/SiO_2 Molar Ratios in Activating Solution	Synthesis Conditions		Compressive Strength (MPa)	Reference
		Temperature (°C)	Ageing Time (Days)		
Brick waste, OPC	0.13	25 ± 3	28	102.6	[3]
Brick waste	0.63	20	7	41.9	[7]
Brick waste, CAC	0.63	65	7	92.0	[38]
Brick waste	0.12	70	28	66.6	[39]
Brick waste, fly ash	1.00	21	28	47.0	[40]
Brick waste, GBFS	0.67	25	28	120.0	[21]
Brick waste, metallurgical slag	0.86	90	7	48.9	This study

[1] OPC: Ordinary Portland cement; CAC: Calcium aluminate cement; GBFS: granulated blast furnace slag.

Robayo-Salazar et al. [3] prepared hybrid cements by mixing ordinary Portland cement (OPC) with brick waste, using as activators, sodium hydroxide and sodium silicate solutions. The produced specimens obtained high compressive strength (102.6 MPa) after curing at room temperature (25 °C) and ageing for 28 days. Fort et al. [7] produced IPs using brick waste as a precursor and mixture of sodium silicate and sodium hydroxide solutions as the alkaline activators. The highest compressive strength obtained for the produced specimens was 41.9 MPa. Reig et al. [38] studied the effect of calcium aluminate cement (CAC) addition during alkali activation with sodium hydroxide and sodium silicate solutions of brick waste. The results showed that the use of CAC accelerates the activation of brick waste and the produced specimens, after curing at 65 °C obtained a maximum compressive strength of 92 MPa. Robayo et al. [39] synthesized IPs based on brick waste using the same activating solutions as in the previously mentioned studies and the specimens acquired compressive strength of 66.5 MPa after curing at 70 °C for 24 h. Rovnanik et al. [40] produced alkali-activated binders by using brick waste and fly ash as precursors, and a mixture of sodium hydroxide and sodium silicate solutions as activators. The produced IPs acquired compressive strength of 47 MPa after curing at room temperature. Rakhimova and Rakhimov [21] prepared IPs from granulated blast furnace slag (GBFS) and brick waste using sodium hydroxide and sodium silicate solutions; after curing at 25 °C, and their compressive strength reached 120 MPa. In the present study, the compressive strength of IPs produced from mixtures of brick waste and metallurgical slag reached 48.9 MPa, after curing at 90 °C for 7 days. Table 5 also shows that the Na_2O/SiO_2 molar ratios in the activating solutions used in all these studies range from 0.12 to 1.

3.3. Morphology of Selected IPs

3.3.1. FTIR Analysis

In order to evaluate the phase transformations that take place between the silicates, calcium and aluminum phases, and the alkaline solutions, FTIR spectra of selected IPs were obtained. Figure 4 shows the FTIR spectra of raw brick and brick-based IPs produced after curing at three different temperatures.

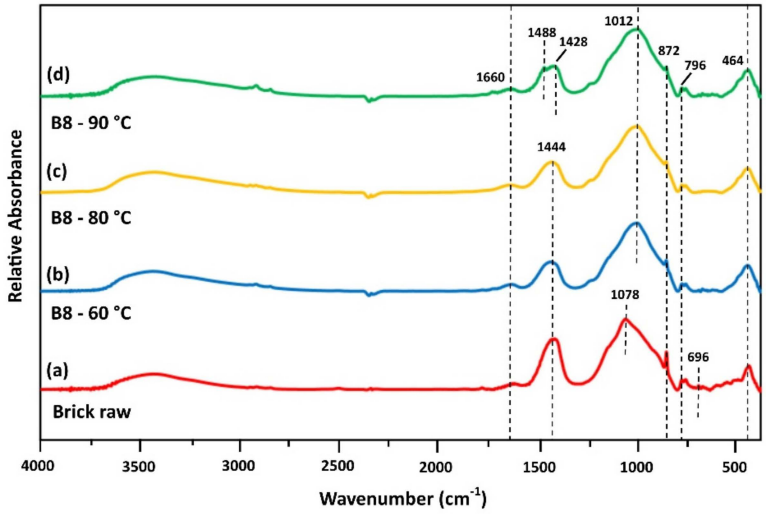

Figure 4. FTIR spectra of (**a**) brick as raw material and brick-based IPs produced after curing at (**b**) 60 °C, (**c**) 80 °C and (**d**) 90 °C (H_2O/Na_2O = 18.2; aged for 7 days).

Brick waste FTIR spectrum is illustrated in Figure 4a. The peak seen at 1660 cm^{-1} is attributed to H–O–H vibration of absorbed water [20]. The bands at ~1444 cm^{-1} and ~872 cm^{-1} are due to C–O stretching and bending and may also indicate that carbonation took place [41,42]. The wide band at 1078 cm^{-1} is primarily due to Si–O bonds and aluminosilicate matrix of brick waste. The relatively intense band at 872 cm^{-1} corresponds to aluminosilicate phase [37]. Si–O and Al–O bonds were also represented as peaks in the range 800–450 cm^{-1} [41,43]. The common differentiation of bands identified in raw brick waste, compared to the bands of brick-based specimens, is related to Si–O bonds (Figure 4a–c). The displacement of band at 1078 cm^{-1} to a lower wavelength (1012 cm^{-1}), indicates the dissolution of aluminosilicate phase present in brick and its polymerization during alkali-activation.

In the spectrum of brick-based specimen (B8), cured at 90 °C (Figure 4d), a shifting of peak at circa 1440 cm^{-1} to a higher wavenumber (1488 cm^{-1}) is observed. This alteration indicates the dissolution of aluminosilicates and existing carbonates (i.e., calcite) from the initial raw material after alkaline activation and their molecular rearrangement to the newly-formed geopolymer gel and carbonates (such as pirssonite), respectively [41,43]. Similarly, a reduction and/or a slight shifting of the bands at 872 cm^{-1} is also observed. These observations comply with compressive strength data, where brick-based specimens cured at 90 °C obtained higher values (43.4 MPa) compared to the ones cured at lower temperatures, 60 °C and 80 °C (13.2 and 27.5 MPa, respectively). The bending vibration at 464 cm^{-1} corresponds to Al–O and Si–O bonds [36].

Figure 5 illustrates the IR spectra of IPs B8, S, B75S25 and B50S50. Slag IP related absorptions are notable at 965 and 510 cm^{-1} (Figure 5b). The band at 510 cm^{-1} is attributed to Fe–O stretching mode due to the presence of magnetite [41,44], while the band at 965 cm^{-1} is assigned to asymmetric stretching Si–O–Si vibrations [37,41]. The peak at 965 cm^{-1} is shifted at 1010 cm^{-1} in B75S25 and B50S50 specimens (Figure 5c,d, respectively). This shift may be attributed to T–O–Si (T = Si or Al) asymmetric stretching vibration occurred in the region (950–1200 cm^{-1}) due to TO_4 reorganization that takes place during IP synthesis [37,41]. In this line of thinking, the new band detected at 1100 cm^{-1} in B75S25 and B50S50 IPs is denoted as the fingerprint of geopolymerization, and indicates the presence of polymeric species with similar chain sizes, while the peak at 965 cm^{-1} in S IP indicates the presence of species of diverse chain sizes [36].

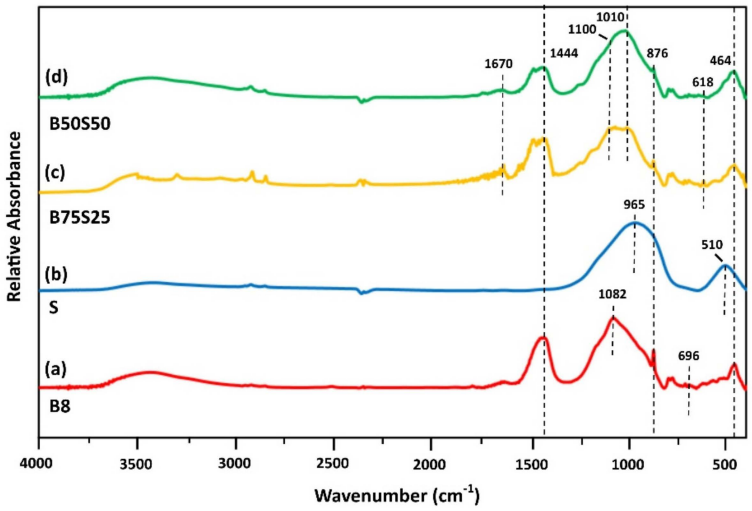

Figure 5. FTIR spectra of IPs (**a**) B8, (**b**) S, (**c**) B75S25 and (**d**) B50S50 (H_2O/Na_2O = 18.2, curing at 90 °C, ageing for 7 days).

3.3.2. Mineralogical Studies

The mineralogy of the IPs produced under the optimum conditions using brick waste (B8) and mixtures of brick waste and slag, B75S25 and B50S50 respectively, along with the XRD patterns of raw brick waste (brick) and slag (slag) are presented in Figure 6.

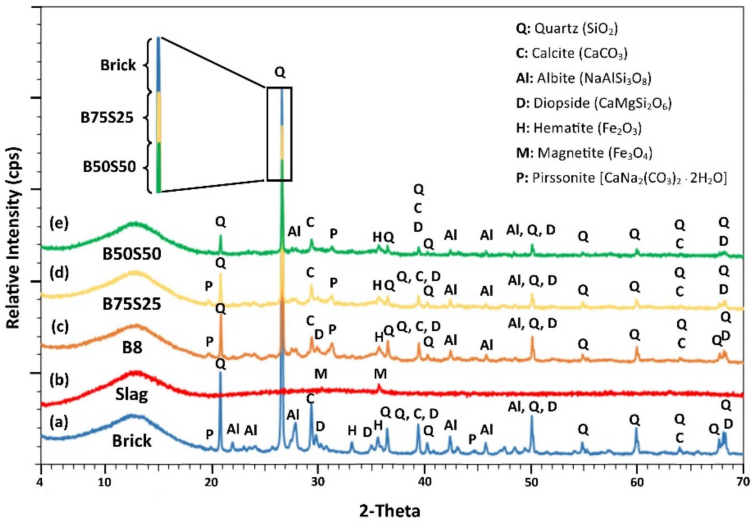

Figure 6. XRD patterns of (**a**) raw brick, (**b**) raw slag as raw materials, and of the IPs produced using (**c**) brick waste (B8), (**d**) 75 wt % brick and 25 wt %. slag (B75S25) and (**e**) 50 wt %. brick and 50 wt % slag (B50S50) under the optimum conditions; i.e., H_2O/Na_2O = 18.21 and curing at T = 90 °C.

Phases such as quartz (SiO_2), calcite ($CaCO_3$), albite ($NaAlSi_3O_8$), diopside ($CaMgSi_2O_6$), pirssonite ($Na_2Ca(CO_3)_2{\cdot}2H_2O$), hematite ($Fe_2O_3$) and magnetite ($Fe_3O_4$) were detected in the raw materials. However, mostly silicate-based phases, namely quartz, diopside and albite, were partially reacted after alkali activation in the examined IPs.

As seen in Figure 6 and especially at the zoom of the primary quartz peak (2-theta = 26.64°), the intensity of the peaks of the crystalline phases present in both brick-based and slag-based specimens are lower than the ones present in the raw materials, while the content of the amorphous phase increases in the produced IPs. This indicates the partial dissolution of crystalline phases after the attack of the raw materials by the activating solution [18]. It should be mentioned here that despite the fact

that the used slag has a relatively high content of Cr_2O_3, previous studies indicated that practically no leaching of Cr from the raw material and the produced IPs takes place [17,24].

3.3.3. SEM Analysis

Figure 7 shows SEM images of selected IPs. No cracks were observed along the cross-sectional interfaces, suggesting the formation of strong bonds due to reactions between the alumino-silicate particles and the alkaline activators (NaOH and Na_2SiO_3 solutions). However, significant differences in the microstructure and the associated EDS analyses were noted among the IPs studied, depending on the starting raw materials. More specifically, the slag-based IP (S) presents a heterogeneous matrix containing large in size, unreacted slag particles; i.e., quartz and magnetite surrounded by an inorganic polymeric gel, consisting of radically dissolved particles after alkali-activation (Figure 7a).

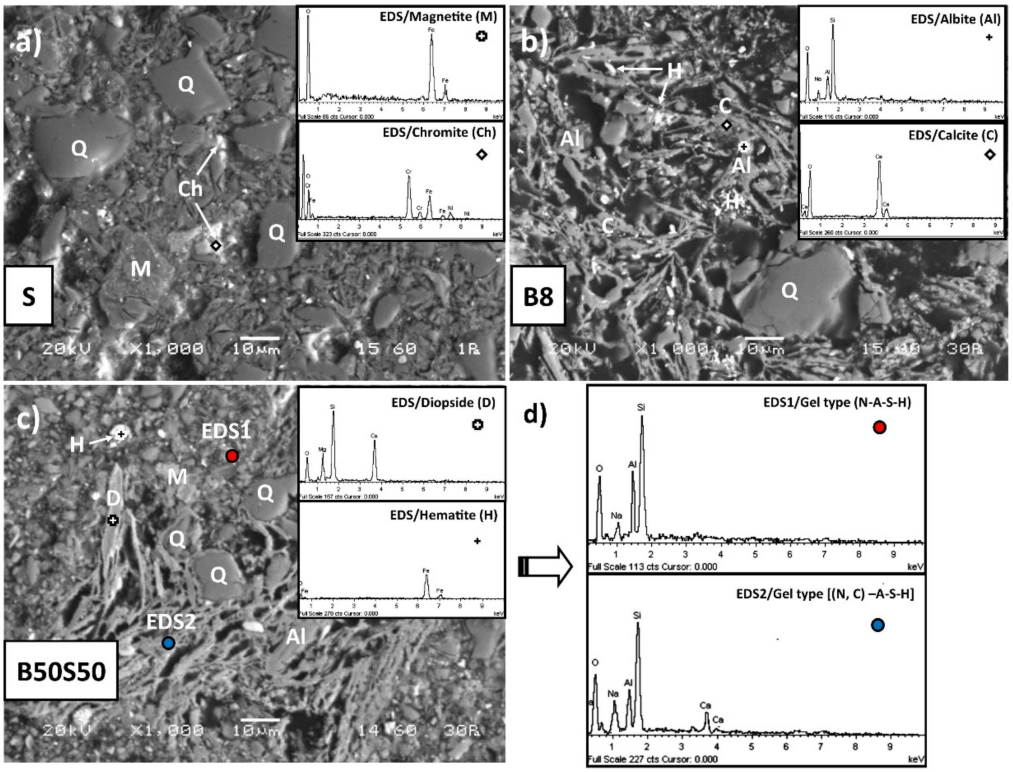

Figure 7. Back-scattered electron images of selected IPs produced with (**a**) metallurgical slag (S), (**b**) brick waste (B8) and (**c**) B50S50 IP specimen. The presence of unreacted minerals is seen in several spot locations in EDS spectra phases (Q: Quartz, C: Calcite, M: Magnetite, H: Hematite, Ch: Chromite, Al: Albite and D: Diopside). (**d**) The formation of gel after alkali-activation of B50S50 (H_2O/Na_2O = 18.2, curing at 90 °C and ageing for 7 days).

On the other hand, the microstructure of the brick-based IPs, namely B8 and B50S50 is mostly characterized by smaller particles and the formation of a more homogenous polymeric network compared to S, as shown in Figure 7b,c, respectively. However, the B50S50 IP is characterized by a more dense and homogeneous gel compared with the IP produced only by brick waste (B8); additionally, fewer unreactive particles, smaller in size, that exhibit better cohesion with the precursors are seen. This microstructure justifies the highest compressive strength obtained for the B50S50 IP (48.9 MPa) (Table 4). The microstructure of the B50S50 IP was further evaluated using quantitative EDS analysis in order to elucidate the formation of the reaction products in the polymeric matrix. SEM-EDS analyses confirmed the formation of two types of gels i.e., N–A–S–H and (N,C)–A–S–H that contained high ratios of Al/Si with values of 0.4 and 0.3, respectively, and a very low Ca/Si value of 0.02. The presence

of these two types of gels detected in the structure of the B50S50 IP justifies its good mechanical properties [45,46].

3.3.4. TG analysis

As seen in Figure 8, at temperatures up to 200 °C, all three IP specimens present a weight loss between 4–5.4% which is attributed to the loss of pore water. The additional mass loss observed at temperatures up to 500 °C is attributed to loss of chemically bound water due to the dehydroxylation of the surface hydroxyl groups OH [47]. The brick-based specimen (Figure 8a) shows additional weight loss (2.9%) at temperatures between 500–700 °C due to calcite decomposition [20].

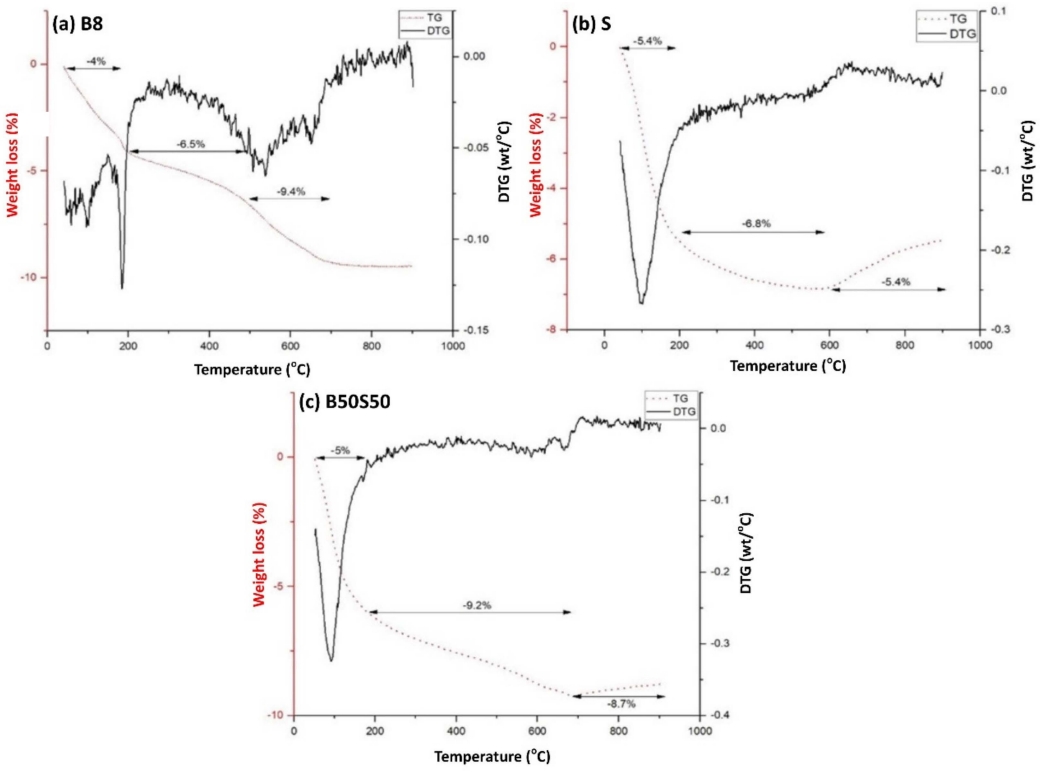

Figure 8. Thermogravimetric (TG) analysis of (**a**) a brick-based specimen (B8), (**b**) a slag-based specimen (S) and (**c**) the B50S50 IP under the optimum synthesis conditions (H_2O/Na_2O = 18.21, curing at 90 °C and ageing for 7 days) (DTG: Derivative thermogravimetric analysis; it is the mass loss rate of sample in g min^{-1} measured by TG analysis).

Concerning slag and brick-slag IPs, mass gain is observed at temperatures higher than 600 °C (Figure 8b,c, respectively). This can be attributed to structural phase transformation of magnetite present in slag and brick-slag IPs. Firstly, maghemite formation takes place as a result of magnetite oxidation at temperatures higher than 120 °C [48] and then, at temperatures higher than 600 °C, the mass gain (S = 1.4%, B50S50 = 0.5%) is due to the structural transition of maghemite to hematite [48,49]. It should be mentioned that magnetite has higher density and hardness compared to maghemite. The kinetics of magnetite-maghemite-hematite transformation is presented in detail in an earlier study [50].

3.4. Durability Performance of Selected IPs

In order to better elucidate the role of synthesis conditions on alkali activation potential, the effect of selected molar ratios of oxides present in the initial paste on the compressive strength of the produced IPs was investigated. IPs produced under the optimal conditions, namely B50S50, using the H_2O/Na_2O molar ratio equal to 18.21 and curing temperature 90 °C, were subjected to firing at higher temperatures,

400, 600 and 800 °C, for 1 h, in a laboratory furnace, and immersed in various solutions; namely distilled water, 1 M HCl and 1 M H_2SO_4, for a period of 7 and 30 days. The aim of these tests was to determine the capability of the produced IPs to withstand high temperature and corrosive environments. The structural integrity of the selected IPs was assessed by means of compressive strength, weight loss and volumetric shrinkage measurements (Table 6).

Table 6. Selected properties of B50S50 IPs fired at high temperatures [1].

Temperature (°C)	Compressive Strength (MPa)	Weight Loss (%)	Shrinkage (%)
90	48.9	-	-
400	39.2	12.1	4.9
600	36.9	12.7	6.0
800	32.5	13.6	7.6

[1] Curing at 90 °C, ageing for 7 days, H_2O/Na_2O = 18.1.

As seen in Table 6, the compressive strength values decrease gradually with the increase in firing temperature. The minimum value of 32.5 MPa, which is still quite high, was obtained for the specimens fired at 800 °C. Moreover, weight loss and volumetric shrinkage increase with the increase in temperature. The lowest weight loss (12.1%) was recorded for the specimens fired at 400 °C, while the highest weight loss (13.6%) was recorded for the specimens fired at 800 °C. Following weight loss, volumetric shrinkage during high temperature firing increased slightly from 4.9% at 400 °C to 7.6% at 800 °C.

Figure 9 illustrates the evolution of compressive strength of B50S50 specimen after immersion in distilled water and acidic solutions (1 M HCl and 1 M H_2SO_4) for 7 and 30 days. It should be mentioned that no buffering of the solution was carried out to better simulate exposure of IPs to phenomena, such as rain or acid rain. Thus, the pHs of the initial solutions, namely distilled water, 1 M HCl and 1 M H_2SO_4, were 7.1, 0.5 and 0.8 respectively, while the pHs after 7 days of immersion were 11.7, 1.5 and 1.2, and after 30 days of immersion increased to 12.3, 2.7 and 1.5, respectively.

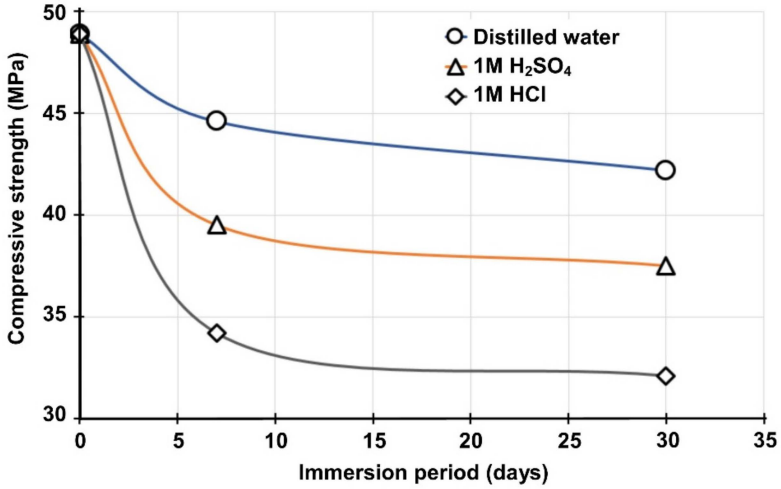

Figure 9. Compressive strength of B50S50 IPs after immersion in distilled water and acidic solutions for 7 and 30 days.

As seen in Figure 9, the greater compressive strength loss (34.3%) was recorded for the specimens immersed in 1 M HCl for 30 days. The specimens immersed in 1 M H_2SO_4 solution for the same period showed also noticeable compressive strength loss (23.3%), whereas the specimens immersed in distilled water for 30 days exhibited the lower loss (13.8%). The reduction in strength is mainly attributed to the disintegration of alumina-silicate bonds, as indicated more clearly by the noticeable pH increase in the case of immersion in 1 M HCl solution [51].

Weight loss and volumetric shrinkage values after immersion in these solutions ranged from 0.5% to 3.5% and 0.7% to 8%, respectively. IPs immersed in HCl solution exhibited the highest weight loss (3.5%) and volumetric shrinkage (8%), while IPs immersed in distilled water exhibited the lowest weight loss (0.5%) and volumetric shrinkage (0.7%). The specimens immersed in HCl and H_2SO_4 solutions for 30 days exhibited different appearances, with softening of their outer surfaces and formations of amorphous silica. In general, it can be concluded that the IPs still retain acceptable to high strength, varying between 32.1 MPa and 37.5 MPa, even when immersed in acidic solutions for a period of 30 days, and a high stability with mass loss lower than 5% in comparison to 30–60% for conventional concrete specimens exposed to acidic environments [51].

Finally, Figure 10 illustrates the compressive strength of B50S50 specimens fired at 800 °C or immersed in distilled water, 1 M HCl and 1 M H_2SO_4 for 30 days and the requirements for load-bearing bricks according to different classification categories (BS 3921:1965). No higher temperature was considered, since after 800 °C, concrete loses its structural integrity [52]. The 7-day compressive strength of B50S50 specimens obtained after curing at 90 °C is also provided, for comparison. It can be seen from this data that B50S50 IP just exceeds the requirements of the demanding Category 7 (48.5 MPa) for load-bearing bricks. Moreover, all produced IPs maintain much sufficient structural integrity even after immersion in acidic solutions (1 M HCl and 1 M H_2SO_4) for 30 days and after high temperature firing at 800 °C, since their final compressive strength values satisfy at least the requirements of Categories 5 (34.5 MPa) and 4 (27.5 MPa), respectively.

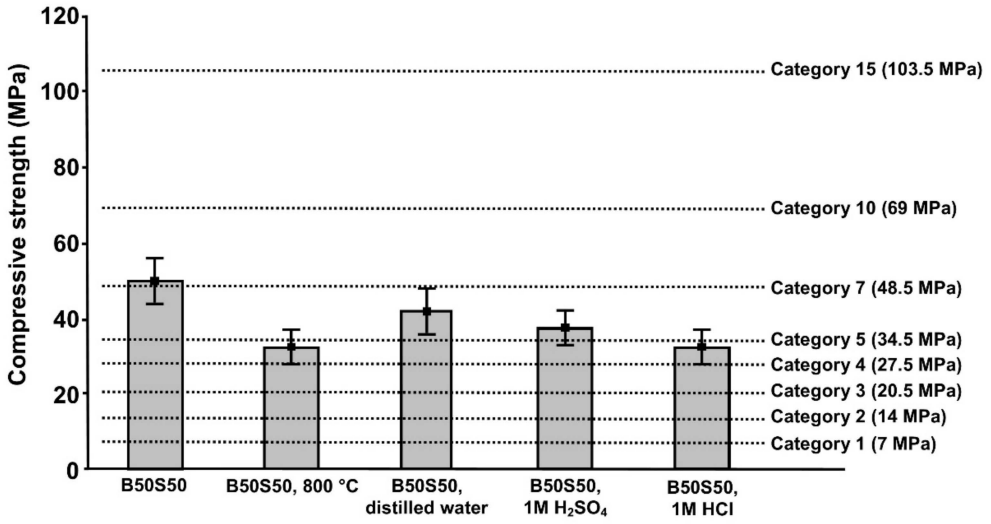

Figure 10. Comparison of the compressive strength of B50S50 specimens (cured at 90 °C), after firing at 800 °C and immersion in distilled water, 1 M HCl and 1 M H_2SO_4, for 30 days, with the values proposed by the different classification categories according to BS 3921:1965 also indicated (error bars represent the standard deviation of three measurements).

4. Conclusions

The present paper shows that brick waste and metallurgical slag can be successfully alkali-activated for the production of IPs with high mechanical strength and good durability performance.

Brick-slag IPs obtained the highest compressive strength (48.9 MPa) when the initial mixture containing equal quantities of each raw material was alkali-activated with a H_2O/Na_2O molar ratio in activating solution equal to 18.1, cured at 90 °C and aged for 7 days. Regarding brick-based IPs, the highest compressive strength (43.4 MPa) was also obtained under the same conditions.

High temperature firing (800 °C) of the produced IPs caused decrease in their compressive strength by 33.5% to 32.5 MPa; however, this value is still considered quite high. The most noticeable effect of acidic attack on IPs was shown after their immersion in 1 M HCl solution for 30 days,

as the compressive strength decreased by 34.4% to 32.1 MPa. On the other hand, specimens immersed in distilled water after 30 days exhibited much higher compressive strength; i.e., 42.2 MPa.

Finally, based on the experimental results, it is deduced that alkali activation is an advantageous process for the co-valorization of large volumes of CDW and metallurgical slags and the production of sustainable building materials or binders with good mechanical properties and durability. However, research efforts should take always into account the high variation in chemical and mineralogical composition of each raw materials' stream that affects their reactivity in alkali-activated systems, thus the quality of the final products.

Author Contributions: K.K. conceived of the idea, designed the experiments, analyzed the results and reviewed the paper. A.S. and A.V. performed the experiments, analyzed the results and wrote the first draft of the paper. G.B. performed the SEM analysis, analyzed the results and reviewed the paper.

Funding: A.S., A.V. and K.K. acknowledge support of this work by the project "INVALOR: Research Infrastructure for Waste Valorization and Sustainable Management" (MIS 5002495), which is implemented under the Action "Reinforcement of the Research and Innovation Infrastructure," funded by the operational program "Competitiveness, Entrepreneurship and Innovation" (NSRF 2014–2020) and co-financed by Greece and the European Union (European Regional Development Fund).

Acknowledgments: The authors wish to express their sincere thanks to the journal editors and two anonymous reviewers for their constructive comments, which significantly improved the quality of the paper.

Conflicts of Interest: The authors declare no conflicts of interest.

References

1. Panizza, M.; Natali, M.; Garbin, E.; Tamburini, S.; Secco, M. Assessment of geopolymers with Construction and Demolition Waste (CDW) aggregates as a building material. *Constr. Build. Mater.* **2018**, *181*, 119–133. [CrossRef]
2. Wong, C.L.; Mo, K.H.; Yap, S.P.; Alengaram, U.J.; Ling, T.C. Potential use of brick waste as alternate concrete-making materials: A review. *J. Clean. Prod.* **2018**, *195*, 226–239. [CrossRef]
3. Robayo-Salazar, R.A.; Rivera, J.F.; de Gutiérrez, R.M. Alkali-activated building materials made with recycled construction and demolition wastes. *Constr. Build. Mater.* **2017**, *149*, 130–138. [CrossRef]
4. Kioupis, D.; Kavakakis, C.; Tsivilis, S.; Kakali, G. Synthesis and characterization of porous fly ash-based geopolymers using Si as foaming agent. *Adv. Mater. Sci. Eng.* **2018**. [CrossRef]
5. Komnitsas, K. Potential of geopolymer technology towards green buildings and sustainable cities. *Procedia Eng.* **2011**, *21*, 1023–1032. [CrossRef]
6. Keawpapasson, P.; Tippayasam, C.; Ruangjan, S.; Thavorniti, P.; Panyathanmaporn, T.; Fontaine, A.; Leonelli, C.; Chaysuwan, D. Metakaolin-Based Porous Geopolymer with Aluminium Powder. *Key Eng. Mater.* **2014**, *608*, 132–138. [CrossRef]
7. Fořt, J.; Vejmelková, E.; Koňáková, D.; Alblová, N.; Čáchová, M.; Keppert, M.; Rovnaníková, P.; Černý, R. Application of waste brick powder in alkali-activated aluminosilicates: Functional and environmental aspects. *J. Clean. Prod.* **2018**, *194*, 714–725. [CrossRef]
8. Ghanbari, M.; Hadiana, A.M.; Nourbakhsh, A.A. Effect of processing parameters on compressive strength of metakaolinite based geopolymers: Using DOE approach. *Procedia Mater. Sci.* **2015**, *11*, 711–716. [CrossRef]
9. Komnitsas, K.; Zaharaki, D.; Perdikatsis, V. Geopolymerisation of low calcium ferronickel slags. *J. Mater. Sci.* **2007**, *42*, 3073–3082. [CrossRef]
10. Komnitsas, K.; Zaharaki, D. Geopolymerisation: A review and prospects for the minerals industry. *Miner. Eng.* **2007**, *20*, 1261–1277. [CrossRef]
11. Hamaideh, A.; Komnitsas, K.; Esaifan, M.; Al-Kafawein, J.K.; Rahier, H.; Alshaaer, M. Advantages of applying a steam curing cycle for the production of kaolinite-based geopolymers. *Arab. J. Sci. Eng.* **2014**, *39*, 7591–7597. [CrossRef]
12. Davidovits, J. Geopolymers and geopolymeric materials. *J. Therm. Anal.* **1991**, *35*, 429–441. [CrossRef]
13. Komnitsas, K.; Zaharaki, D.; Vlachou, A.; Bartzas, G.; Galetakis, M. Effect of synthesis parameters on the quality of construction and demolition wastes (CDW) geopolymers. *Adv. Powder Technol.* **2015**, *26*, 368–376. [CrossRef]

14. Alshaaer, M.; Zaharaki, D.; Komnitsas, K. Microstructural characteristics and adsorption potential of zeolitic tuff-metakaolin geopolymers. *Desal. Water Treat.* **2015**, *56*, 338–345. [CrossRef]
15. Arnold, M.C.; de Vargas, A.S.; Bianchini, L. Study of electric-arc furnace dust (EAFD) in fly ash and rice husk ash-based geopolymers. *Adv. Powder Technol.* **2017**, *28*, 2023–2034. [CrossRef]
16. Xia, M.; Muhammad, F.; Zeng, L.; Li, S.; Huang, X. Solidification/stabilization of lead-zinc smelting slag in composite based geopolymer. *J. Clean. Prod.* **2019**, *209*, 1206–1215. [CrossRef]
17. Komnitsas, K.; Zaharaki, D.; Bartzas, G. Effect of sulphate and nitrate anions on heavy metal immobilisation in ferronickel slag geopolymers. *Appl. Clay Sci.* **2013**, *73*, 103–109. [CrossRef]
18. Zaharaki, D.; Komnitsas, K.; Perdikatsis, V. Use of analytical techniques for identification of inorganic polymer gel composition. *J. Mater. Sci.* **2010**, *45*, 2715–2724. [CrossRef]
19. Bernal, S.A.; Rodríguez, E.D.; Kirchheim, A.P.; Provis, J.L. Management and valorisation of wastes through use in producing alkali-activated cement materials. *J. Chem. Technol. Biotechnol.* **2016**, *91*, 2365–2388. [CrossRef]
20. Zaharaki, D.; Galetakis, M.; Komnitsas, K. Valorization of construction and demolition (C&D) and industrial wastes through alkali activation. *Constr. Build. Mater.* **2016**, *121*, 686–693. [CrossRef]
21. Rakhimova, N.R.; Rakhimov, R.Z. Alkali-activated cements and mortars based on blast furnace slag and red clay brick waste. *Mater. Des.* **2015**, *85*, 324–331. [CrossRef]
22. Komnitsas, K. Co-valorization of marine sediments and construction & demolition wastes through alkali activation. *J. Environ. Chem. Eng.* **2016**, *4*, 4661–4669. [CrossRef]
23. Xu, H.; Van Deventer, J.S.J. The geopolymerisation of alumino-silicate minerals. *Int. J. Miner. Process.* **2000**, *59*, 247–266. [CrossRef]
24. Liu, Z.; El-Tawil, S.; Hansen, W.; Wang, F. Effect of slag cement on the properties of ultra-high performance concrete. *Constr. Build. Mater.* **2018**, *190*, 830–837. [CrossRef]
25. Bougara, A.; Lynsdale, C.; Neil, B.; Milestone, N.B. The influence of slag properties, mix parameters and curing temperature on hydration and strength development of slag/cement blends. *Constr. Build. Mater.* **2018**, *187*, 339–347. [CrossRef]
26. Zaharaki, D.; Komnitsas, K. Effect of additives on the compressive strength of slag-based inorganic polymers. *Glob. Nest J.* **2009**, *11*, 137–146. [CrossRef]
27. Perera, D.S.; Cashion, J.D.; Blackford, G.M.; Zhang, Z.; Vance, E.R. Fe speciation in geoplymers with Si/Al molar ratio of ~2. *J. Eur. Ceram. Soc.* **2007**, *27*, 2697–2703. [CrossRef]
28. Lemougna, P.N.; MacKenzie, K.J.D.; Jameson, G.N.L.; Rahier, H.; Chinje Melo, U.F. The role of iron in the formation of inorganic polymers (geopolymers) from volcanic ash: A ^{57}Fe Mössbauer spectroscopy study. *Int. J. Mater. Sci.* **2013**, *48*, 5280–5286. [CrossRef]
29. Peys, A.; White, C.E.; Rahier, H.; Blanpain, B.; Pontikes, Y. Alkali-activation of CaO-FeOx-SiO_2 slag. Formation mechanism from in-situ X-ray total scattering. *Cem. Concr. Res.* **2019**, *122*, 179–188. [CrossRef]
30. Akcil, A.; Agcasulu, I.; Swain, B. Valorization of waste LCD and recovery of critical raw material for circular economy: A review. *Resour. Conserv. Recy.* **2019**, *149*, 622–637. [CrossRef]
31. Baldassarre, B.; Schepers, M.; Bocken, N.; Cuppen, E.; Korevaar, G.; Calabretta, G. Industrial Symbiosis: Towards a design process for eco-industrial clusters by integrating Circular Economy and Industrial Ecology perspectives. *J. Clean. Prod.* **2019**, *216*, 446–460. [CrossRef]
32. Komnitsas, K.; Bartzas, G.; Karmali, V.; Petrakis, E.; Kurylak, W.; Pietek, G.; Kanasiewicz, J. Assessment of Alkali Activation Potential of a Polish Ferronickel Slag. *Sustainability* **2019**, *11*, 1863. [CrossRef]
33. *EN 13755, Natural Stone Test Methods—Determination of Water Absorption at Atmospheric Pressure*; British Standards Institution: London, UK, 2008.
34. Tuyan, M.; Andiç-Çakir, Ö.; Ramyar, K. Effect of alkali activator concentration and curing condition on strength and microstructure of waste clay brick powder-based geopolymer. *Compos. Part B Eng.* **2018**, *135*, 242–252. [CrossRef]
35. Vásquez, A.; Cárdenas, V.; Robayo, R.A.; de Gutiérrez, R.M. Geopolymer based on concrete demolition waste. *Adv. Powder Technol.* **2016**, *27*, 1173–1179. [CrossRef]
36. Maragkos, I.; Giannopoulou, I.P.; Panias, D. Synthesis of ferronickel slag-based geopolymers. *Miner. Eng.* **2009**, *22*, 196–203. [CrossRef]
37. Komnitsas, K.; Zaharaki, D.; Perdikatsis, V. Effect of synthesis parameters on the compressive strength of low-calcium ferronickel slag inorganic polymers. *J. Hazard. Mater.* **2009**, *161*, 760–768. [CrossRef]

38. Reig, L.; Soriano, L.; Borrachero, M.V.; Monzo, J.; Paya, J. Influence of calcium aluminate cement (CAC) on alkaline activation of red clay brick waste (RCBW). *Cem. Concr. Compos.* **2016**, *65*, 177–185. [CrossRef]
39. Robayo, R.; Mulford, A.; Munera, J.; Mejia de Gutiérrez, R. Alternative cements based on alkali-activated red clay brick waste. *Constr. Build. Mater.* **2016**, *128*, 163–169. [CrossRef]
40. Rovnanik, P.; Reznik, B.; Rovnanikovà, P. Blended alkali-activated fly ash/brick powder materials. *Proc. Eng.* **2016**, *151*, 108–113. [CrossRef]
41. Socrates, G. *Infrared and Raman Characteristic Group Frequencies*, 3rd ed.; John Wiley & Sons Ltd.: Chichester, UK, 2001.
42. Yu, P.; Kirkpatrick, R.J.; Poe, B.; Mcmillan, P.F.; Cong, X. Structure of Calcium Silicate Hydrate (C–S–H): Near-, Mid-, and Far-Infrared Spectroscopy. *J. Am. Ceram. Soc.* **1999**, *18*, 742–748. [CrossRef]
43. Gervais, F.; Blin, A.; Massiot, D.; Coutures, J.P.; Chopinet, M.H.; Naudin, F. Infrared reflectivity spectroscopy of silicate glasses. *J. Non Cryst. Solids* **1987**, *89*, 384–401. [CrossRef]
44. Muthuvel, I.; Gowthami, K.; Thirunarayanan, G.; Suppuraj, P.; Krishnakumar, B.; do Nascimento Sobral, J.F.; Swaminathan, M. Graphene oxide–$Fe_2V_4O_{13}$ hybrid material as highly efficient hetero-Fenton catalyst for degradation of methyl orange. *Int. J. Ind. Chem.* **2019**, *10*, 1–11. [CrossRef]
45. Sedira, N.; Castro-Gomes, J.; Magrinho, M. Red clay brick and tungsten mining waste-based alkali-activated binder: Microstructural and mechanical properties. *Constr. Build. Mater.* **2018**, *190*, 1034–1048. [CrossRef]
46. Jena, S.; Panigrahi, R. Performance assessment of geopolymer concrete with partial replacement of ferrochrome slag as coarse aggregate. *Constr. Build. Mater.* **2019**, *220*, 525–537. [CrossRef]
47. Dimas, D.; Giannopoulou, I.; Panias, D. Polymerization in sodium silicate solutions: A fundamental process in geopolymerization technology. *J. Mater. Sci.* **2009**, *44*, 3719–3730. [CrossRef]
48. Vergés, M.A.; Costo, R.; Roca, A.G.; Marco, J.F.; Goya, G.F.; Serna, C.J.; Morales, M.P. Uniform and water stable magnetite nanoparticles with diameters around the monodomain-multidomain limit. *J. Phys. D Appl. Phys.* **2008**, *41*, 134003–134022. [CrossRef]
49. Ye, X.; Lin, D.; Jiao, Z.; Zhang, L. The thermal stability of nanocrystalline maghemite. *J. Phys. D Appl. Phys.* **1998**, *31*, 2739–2744. [CrossRef]
50. Swaddle, T.W.; Oltmann, P. Kinetics of the magnetite-maghemite-hematite transformation, with special reference to hydrothermal systems. *Can. J. Chem.* **1980**, *58*, 1763–1772. [CrossRef]
51. Mehta, A.; Siddique, R. Sulfuric acid resistance of fly ash based geopolymer concrete. *Constr. Build. Mater.* **2017**, *146*, 136–143. [CrossRef]
52. Lahoti, M.; Tan, K.H.; Yang, E.-H. A critical review of geopolymer properties for structural fire-resistance applications. *Constr. Build. Mater.* **2019**, *221*, 514–526. [CrossRef]